Applied Catalysis B: Environmental 84 (2008) 125–132

Contents lists available at ScienceDirect

Applied Catalysis B: Environmental

journal homepage: www.elsevier.com/locate/apcatb

Multi-step loading of titania on mesoporous silica: Influence of the morphology and the porosity on the catalytic degradation of aqueous pollutants and VOCs

K. De Witte [a,*], V. Meynen [a,b], M. Mertens [b], O.I. Lebedev [c], G. Van Tendeloo [c], A. Sepúlveda-Escribano [d], F. Rodríguez-Reinoso [d], E.F. Vansant [a], P. Cool [a]

[a] University of Antwerpen, Laboratory of Adsorption and Catalysis, Universiteitsplein 1, B-2610 Wilrijk, Belgium
[b] Flemish Institute for Technological Research (VITO), Boeretang 200, B-2400 Mol, Belgium
[c] University of Antwerpen, EMAT, Groenenborgerlaan 171, B-2020 Antwerpen, Belgium
[d] Universidad de Alicante, Departamento de Química Inorgánica, Apartado 99, 03080 Alicante, Spain

ARTICLE INFO

Article history:
Received 30 January 2008
Received in revised form 13 March 2008
Accepted 15 March 2008
Available online 4 April 2008

Keywords:
Titania
ACSG
Silica
Photocatalysis
Gaseous phase
Aqueous phase
Morphology

ABSTRACT

Titania nanoparticles have been deposited on inert porous silica supports with high specific surface area. These materials have potential applications in paint and textile industry as the titania particles selectively deposited on the inner surface of the silica supports act as a photocatalyst. The inert external surface is necessary to avoid photodegradation of the textile material or the paint components. The photocatalytic activity of the catalysts has been evaluated with two catalytic setups. One setup in aqueous phase, for the degradation of dyes such as rhodamine-6G, is commonly used. The second setup is a continuous flow gaseous phase setup which was used for the mineralization of ethanol as a representative volatile organic compound (VOC). The influence of the porosity and the morphology of the silica supports on the photocatalytic activity are discussed.

1. Introduction

The last years, more and more studies have been carried out demonstrating bad indoor air quality in the majority of homes and offices [1–4]. This bad air quality has a negative impact on human health and is linked to the presence of volatile organic compounds (VOCs) [5–9]. Indoor sources of pollutants are numerous. For example, building materials can give rise to VOCs exceeding the recommended maximum indoor levels [10]. Also common indoor activities, such as cooking and cigarette smoking generate pollutants. An attractive route to improve the indoor air quality is to adsorb and catalytically degrade the pollutants [11,12]. This functionality can be integrated into the decoration elements such as carpets and curtains. Therefore the catalyst has to be embedded into the textile fibers, requesting several demands for the catalyst. The particle size of the catalyst has to be small enough to fit in the textile fibers without decreasing the strength of the fibers. Moreover, the external surface of the catalyst needs to be inactive to prevent degradation of the organic textile fibers and colors after a short period of time. Finally, the catalytic activity needs to be high enough to be able to degrade the VOCs.

Titania is a widely investigated semiconductor and its good photocatalytic activity towards the degradation of organic compounds has been demonstrated [13–15]. In this way, titania is a good candidate for the photocatalytic removal of VOCs in indoor air in order to improve its quality [16–19].

In this work, catalytic active titania is deposited on the internal surface of inert mesoporous silica supports leaving the external surface inert [20]. The efforts made on the synthesis of these mesoporous siliceous materials resulted in a wide range of materials with different pore structures, pore diameters, stabilities and adsorption capacities. One of these materials is SBA-15, which was first synthesized by Zhao et al. [21,22]. It is one of the most intensively studied mesoporous silica supports due to its easy synthesis, controllable and uniform pore dimensions and its good thermal and hydrothermal stability.

As stated above, the particle size of the final catalyst must be small enough to fit into the textile fibers. Therefore, several

* Corresponding author. Tel.: +32 3 820 23 54; fax: +32 3 820 23 74.
E-mail address: koen.dewitte@ua.ac.be (K. De Witte).

0926-3373/$ – see front matter © 2008 Elsevier B.V. All rights reserved.
doi:10.1016/j.apcatb.2008.03.015

adjustments were implemented in the original synthesis procedure of the SBA-15 support material. First, rod-like SBA-15 was synthesized to decrease the particle size of this inert support [23–25]. In a next step, a swelling agent was added during the synthesis, resulting in a mesocellular foam structure with a high surface area, large pore radius, high pore volume and small particle size [26–28].

For the incorporation of titania in mesoporous silica, several methods have been studied. One way to combine mesoporous silica with titania active centers is to synthesize the siliceous support material and subsequently deposit titania on its surface by applying post-synthesis methods [29–31]. Methods like grafting, impregnation, ACSG (acid-catalyzed sol–gel), etc., are commonly used [32,33]. A second approach to form titania-activated mesoporous silica is by introducing titania by an in situ method [34–37]. Thereby, the titania–silica composites are synthesized by homogeneously mixing suitable precursors. In this way, Ti atoms are incorporated in the silica structure during the formation of the mesoporous material. By applying these in situ methods, it is expected to incorporate titania in the silica matrix rather than on the silica surface as is the case for post-synthetic deposition methods.

In this work, the post-synthesis acid-catalyzed sol–gel method [38] was used to deposit titania nanoparticles into the mesopores of the silica support materials. In a multi-step deposition, the loading of titania was systematically increased without blocking of the mesopores [20]. Here, we report the multi-step impregnation of titania nanoparticles in several mesoporous siliceous support materials with different structural features. The emphasis is put on the preparation of catalysts with inert external surfaces for textile, wallpaper and paint industry. Special attention is given to the particle size and pore size of the support materials. The influence of the structural differences on the changes in catalytic performance and its relation to diffusion aspects is studied. Suitable catalysts are obtained that can be applied in the textile industry.

2. Experimental

2.1. Chemicals

Tetraethoxysilane (Acros), mesitylene (1,3,5-trimethylbenzene) (Acros), hydrogen chloride (37%) (Acros) and pluronic P123 ($EO_{20}PO_{70}EO_{20}$) (Aldrich) were used for the synthesis of SBA-15 and MCF. Titanium tetra isopropoxide (Aldrich), nitric acid (65%) (Acros) and NaOH pellets (Acros) were utilized for the preparation of the catalysts. Rhodamine-6G, a dye for the catalytic experiments was purchased from Acros.

2.2. Synthesis of the support materials

2.2.1. Santa Barbara acid (SBA)-15 [20,21]

SBA-15 was prepared following a method reported by Zhao et al. First, 4 g of P123 was dissolved in 20 ml HCl and 130 ml H_2O. This solution was heated to 45 °C and then 9.14 ml of TEOS was added and stirred at this temperature for 7.5 h. Subsequently, the solution was aged at 80 °C for 15.5 h. Afterwards the obtained material was filtered, washed and calcined at 550 °C for 6 h with a heating rate of 1 °C/min.

2.2.2. Mesocellular foams (MCF) [25,26]

As in the synthesis of SBA-15, 4 g of P123 was dissolved in 130 ml H_2O and 20 ml HCl. But after the dissolving of the surfactant, 0.0467 g of NH_4F and 4.6 ml of a swelling agent (mesitylene) were added. After 1 h, 9.14 ml of TEOS was added and stirred for 20 h at 45 °C. Subsequently, an ageing process was carried out in an autoclave at 100 °C for 24 h. Afterwards, the sample was filtered, washed and calcined at 550 °C for 6 h with a heating rate of 1 °C/min.

2.2.3. SBA short-channel (sc) [22–24]

For the synthesis of SBA sc, 4 g P123 was dissolved in 20 ml HCl and 130 ml H_2O. This solution was heated to 40 °C. After the addition of 7.5 ml of TEOS, the solution was stirred for 8 min and further aged for 24 h at 40 °C under static conditions. Then a second ageing step was carried out in an autoclave for 24 h at 100 °C. In a last step, the silica material was filtered, washed with H_2O and calcined at 550 °C for 6 h with a heating rate of 1 °C/min.

2.2.4. SBA short-channel, swelling agent (scs) [27]

SBA scs was synthesized by dissolving 4 g P123 in 20 ml HCl and 130 ml H_2O. To this solution, 2.2 g of KCl and 5 ml of mesitylene was added and heated to 40 °C. Then, 10 ml of TEOS was added and the solution was stirred for 8 min. After ageing for 24 h at 40 °C and 24 h at 100 °C in an autoclave, the sample was filtered, washed with H_2O and calcined at 550 °C for 6 h with a heating rate of 1 °C/min.

2.3. Synthesis of the catalysts

The catalysts were synthesized by the acid-catalyzed sol–gel method. Titanium tetra isopropoxide was added gradually (0.5 ml/5 min) to an aqueous solution of HNO_3 under continuous stirring. Depending on the loading of TiO_2 on the catalyst, the requisite amounts of titanium tetra isopropoxide were added. After 2 h of stirring, a transparent sol with titania nanoparticles was obtained. The transparent sol was diluted with de-ionized water and the pH was adjusted to 3 by addition of the necessary amount of a 1 M NaOH solution. Then, 0.5 g of the support material was added to the suspension and stirred for another 2 h. The Ti-activated material was collected by several centrifugations and washing cycles with de-ionized water until pH 6. After drying and calcination in air at 300 °C for 2 h, the titania-based catalyst was obtained. This loading procedure was repeated more than once in order to deposit higher amounts of titania [20]. Obtained samples are designated as silica-*i*-*j*, where *i* is the number of loading cycles and *j* means the amount (ml) of titanium tetra isopropoxide added in each loading cycle.

2.4. Characterization

Nitrogen adsorption/desorption isotherms at −196 °C were performed on a Quantachrome Autosorb-1-MP automated gas adsorption system. The isotherms were measured after outgassing of the samples under vacuum for 16 h at 200 °C. The Brunauer–Emmet–Teller (BET) method was used to calculate the specific surface area. The pore diameter was obtained using the Barret–Joyner–Halenda (BJH) method and the total pore volume was determined at $P/P_0 = 0.95$.

The crystal phase of the titania nanoparticles was determined by FT-Raman spectroscopy. The spectra were measured on a Nicolet Nexus FT-Raman spectrometer with a Ge detector and a 1064 nm Nd:YAG laser. Samples were measured in a 180° reflective sampling configuration. Five hundred scans were averaged for each sample and the laser power was set between 0.5 and 1 W.

Scanning electron microscopy (SEM) was performed using a JSEM 5510 system operating at an accelerating voltage of 15 kV. The samples were sputtered with a thin film of gold to minimize the charging effects.

Conventional transmission electron microscopy (TEM) was performed on a Philips CM20 operated at 200 kV with a point resolution of 0.27 nm and equipped with a fiber optic-coupled GATAN 622 TV system. The crushed crystallites were deposited on a holly carbon grid before measurement. Low electron beam intensities and lower magnification were applied in order to

preserve the structure and to avoid sample drift during the exposure of the films. High-angle annular dark-field (HAADF) scanning TEM (STEM) experiments were performed using a JEOL 3000F TEM/STEM electron microscope having a 0.2 nm STEM resolution.

The Ti-loading on the support was determined by electron probe microanalysis measurements (EPMA). The measurements were carried out on a JEOL JXA-733 apparatus.

X-ray diffractograms (XRD) were collected on a Panalytical X'Pert PRO MPD diffractometer using Ni-filtered Cu Kα radiation. Measurements were done in the 2θ mode using a bracket sample holder with a scanning speed of 0.04°/4s continuous mode.

The photocatalytic activity of the catalysts in the liquid phase was tested by photodegradation of rhodamine-6G in aqueous solution. 25 mg of the catalyst was added to a solution of rhodamine-6G (25 ml, 4×10^{-5} M) and stirred for half an hour in the absence of UV irradiation in order to establish an adsorption/desorption equilibrium between rhodamine-6G and the surface of the catalyst. Then, the solution was illuminated for 1 h with UV-light (100 W Hg-lamp, 365 nm, Sylvania Par 38). During this illumination period, samples (5 ml) of the suspension were collected at fixed time intervals (10 min) and analyzed by UV–vis spectroscopy (Thermo-electron evolution 500, double beam UV–vis spectrometer). The absorbance was measured at 526 nm with water as a reference and converted to concentration using the Lambert–Beer's law. The adsorption and catalysis are recalculated to percentages.

The photocatalytic activity in gaseous environment was tested in a continuous gas flow setup (Fig. 8) and analysed with a GC apparatus (Agilent) equipped with a FID detector and a HP5 capillary column.

3. Results and discussion

3.1. Support materials

The siliceous support materials have to fulfill several demands before they can be applied in the textile industry. Following an extrusion process, the materials will be dispersed in the textile fibers. Therefore the particle size of the materials has to be smaller than 2 μm in order to preserve the strength of the textile fibers. On the other hand, the pore radius and the pore volume of the materials have to be sufficient to allow diffusion of volatile organic compounds and activation with photocatalytic active elements. Several siliceous support materials (SBA-15, MCF, SBA sc and SBA scs) were therefore synthesized, as described in Section 2, and compared. SBA-15 and MCF were synthesized as described in literature [20,21,25,26]. The syntheses of SBA sc and SBA scs here reported are the result of a parameter study on an earlier optimization of the synthesis procedures [22–24,27].

Table 1
Structural and elemental properties of the different materials

Sample	Ti (wt.%)	S_t (m^2/g)	V_t (ml/g)	r (Å)	S_μ (m^2/g)	V_μ (ml/g)
SBA-15	0	719	0.8	27	290	0.127
MCF	0	583	2.2	83	166	0.07
SBA sc	0	729	1.4	37	117	0.04
SBA scs	0	421	2.0	72	51	0.014
SBA-3-2	47.3	322	0.41	18–27	0	0
MCF-3-2	48.1	236	0.44	27–83	2.4	0
SBAsc-3-2	48.8	226	0.38	23–37	2.2	0
SBAscs-3-2	45.0	196	0.53	27–72	0	0

S_t: specific surface area; V_t: total pore volume; R: pore radius; S_μ: microporous surface area; V_μ: micropore volume.

Fig. 1 and Table 1 show the data collected from the N_2-sorption isotherms at −196 °C. All isotherms are of type IV, characteristic for mesoporous materials. SBA-15 as well as SBA sc show a typical isotherm for materials with ordered mesoporous channels. Nevertheless, the hysteresis of SBA sc is shifted to higher relative pressure compared to the normal SBA-15, indicating that larger pores are obtained. Also the pore volume is slightly higher than the pore volume of SBA-15. Both materials have a high specific surface area. The materials synthesized using a swelling agent (MCF and SBA scs) show typical isotherms for materials with high pore volumes and large pore radii. The hysteresis loop appears at high relative pressures and at this point, the isotherms show a large increase in the amount of adsorbed nitrogen. On the other hand, these materials have smaller specific surface areas. SBA scs, in comparison to MCF, has a broader pore size distribution, a slightly lower specific surface area and total pore volume and smaller pore dimensions. Moreover, the micropore volume and micropore surface area is much less than in all other support materials. All

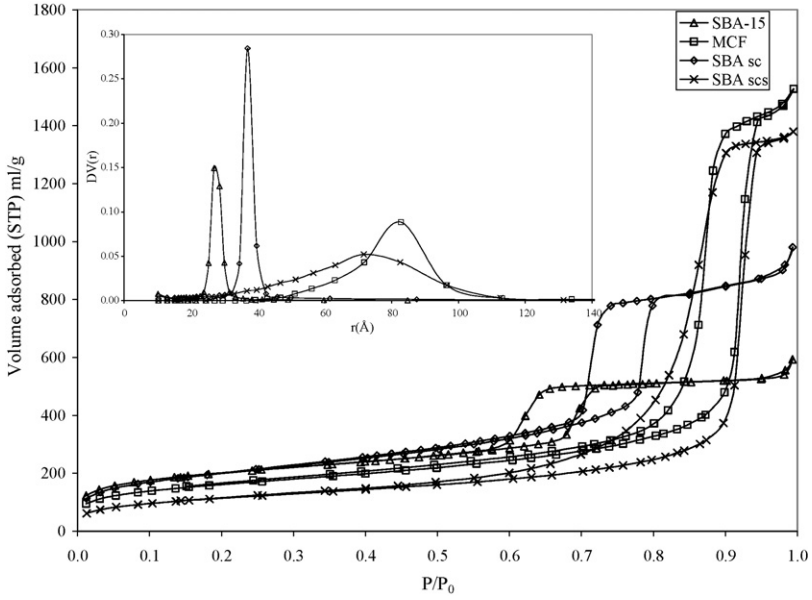

Fig. 1. N_2-sorption isotherms of the different mesoporous silica supports at −196 °C. (Inset) Pore size distribution of the siliceous supports.

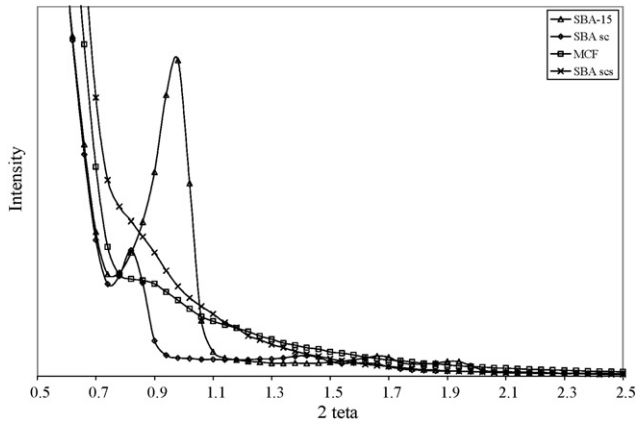

Fig. 2. XRD patterns of the mesoporous silica supports.

four materials have a hexagonal ordering, as can be seen in XRD (Fig. 2). SBA-15 and SBA sc show clear signals of hexagonal ordering represented by the (1 0 0), (1 1 0) and (2 0 0) peaks. A clear shift to smaller angles 2θ can be observed for SBA sc due to its larger pore dimensions. The radii of SBA scs and MCF are even larger. Therefore, the XRD peaks shift to smaller angles 2θ and the (1 0 0) signals are beneath the detection limit leaving only the (1 1 0) and (2 0 0) peaks to be observed. Fig. 3 shows the SEM images of the different materials. SBA-15 consists of long fibers of up to 100 μm in length (Fig. 3a). When swelling agents are applied (MCF and SBA scs), the fibrous structure disappears and smaller, more spherical, agglomerated structures are formed. Short-channel SBA (SBA sc, Fig. 3c) has a rod-like structure with particle dimensions of 0.3–1.2 μm. They are similar in shape as the fibrous structure, but much shorter in length and less aggregated. The same results are observed when similar materials with the addition of swelling agents are studied (Fig. 3d). Short-channel structures such as SBA scs show smaller particles that are less aggregated. As can be seen, only SBA sc and SBA scs have particle sizes that are satisfactory to meet the interest of the textile industry. The more commonly used SBA-15 and MCF with larger particles will be further used as reference materials to study the morphological effect on the catalytic performance.

3.2. Characterization of the catalyst

Several catalysts were prepared starting from four different support materials and following the ACSG deposition method as described in Section 2. The results of the multi-step deposition process of titania on SBA-15 were reported earlier [20]. These results indicate that SBA-3-2 (three loading cycles of 2 ml $Ti(O^iPr)_4$) is the most photoactive catalyst in the reported series (ACSG method on SBA-15). The three other support materials (MCF, SBA sc and SBA scs) were synthesized and characterized in the same way and similar results are obtained. Therefore, in this work, the most photoactive catalysts (SBA-3-2, MCF-3-2, SBA sc-3-2 and SBA scs-3-2) will be compared and discussed.

3.2.1. N_2-sorption isotherms at −196 °C

The N_2-sorption isotherms of the four catalysts are given in Fig. 4 and the deducted data are shown in Table 1. A loss in pore volume and surface area is obtained for all the materials after deposition of the titania nanoparticles. This is due to: (1) the titania particles deposited in the mesopores of the silica materials will block the micropores. This results in a significant decrease in microporous-specific surface area and pore volume. For example

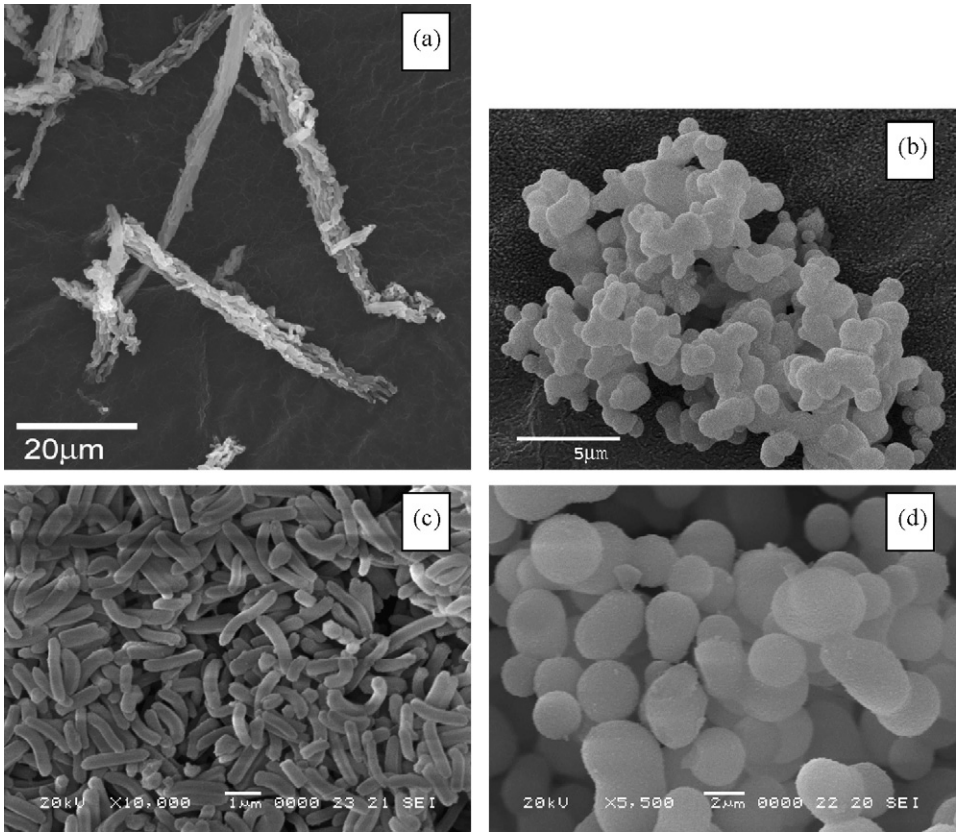

Fig. 3. SEM images of the mesoporous silica supports: (a) SBA-15, (b) MCF, (c) SBA sc and (d) SBA scs.

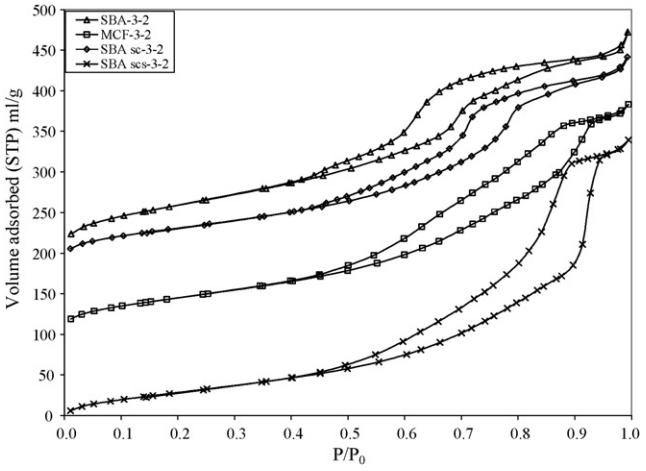

Fig. 4. N_2-sorption isotherms of the catalysts. Offsett: SBA-3-2 = 170, MCF-3-2 = 80, SBA sc-3-2 = 170 and SBA scs-3-2 = −25.

SBA-15, with a microporous surface area of 290 m^2/g, shows no microporosity after deposition of titania particles (SBA-3-2). (2) The titania nanoparticles occupy a part of the mesopores resulting in a decreased pore volume. (3) Keeping in mind the higher molecular weight of titania in comparison to silica and the titanium weight percentages of up to 49 wt.%, one can conclude that the specific surface area and the total pore volume (both expressed per gram) will be seriously decreased. The two SBA type catalysts (SBA-3-2 and SBA sc-3-2) show two significant differences in isotherm shape with respect to the parent support materials SBA-15 and SBA sc, respectively. In the relative pressure region beneath the hysteresis of the support material (0.4–0.6 and 0.5–0.7 P/P_0, respectively), an extra desorption step occurs. This second desorption step is due to the presence of the titania nanoparticles present in the mesopores of the support materials. [39] The narrowed pores, formed between two nanoparticles, are only desorbed at lower relative pressure and therefore a second desorption step appears. The narrowed pores are originating from the titania nanoparticles that are randomly deposited in the mesopores of the materials, therefore narrowing the pores in several places. As a result, a bimodal pore size distribution has been obtained by the BJH method. One of the pore radii corresponds to the pore radius of the mesoporous support material and thus belongs to the remaining open pores. The other pore radius is smaller and is caused by the narrowing of the pores through deposition of the titania nanoparticles inside the mesopores of the support.

A second difference in the isotherms shape of SBA-3-2 and SBA sc 3-2 compared to those of the parent support material is noticed in the higher relative pressure region (above 0.7 and 0.8 P/P_0, respectively). Here, the adsorption and the desorption branch do not close at the same relative pressure as in the parent material. The delayed closing of the hysteresis is an indication for the formation of extra pores with larger pore radii. Therefore, although the effect is small, it is clear that extra porosity is created at the external surface of the support material and as a consequence of titania nanoparticles that are deposited as well at the internal surface as at the external surface of the support material. [40] The catalysts prepared with the addition of swelling agents (MCF-3-2 and SBA scs-3-2) show similar differences such as postponed desorption and closure of the hysteresis loop to lower P/P_0 volumes, compared to their support materials (MCF and SBA scs, respectively). Therefore also in these materials, the presence of narrowed mesopores can give evidence for the deposition of titania

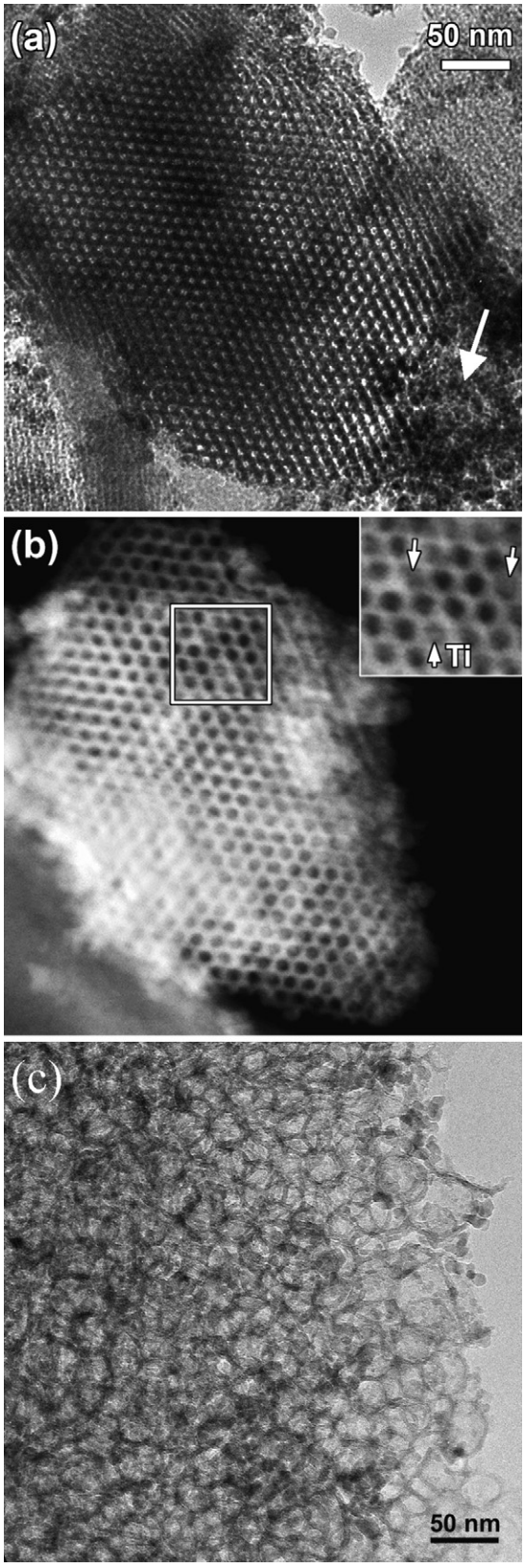

Fig. 5. TEM images of (a) SBA sc-3-2, (b) SBA sc-3-2 measured with z-contrast and (c) SBA scs-3-2.

nanoparticles at the internal surface. However, the closing of the hysteresis in the higher relative pressure region stays unaltered. This observation indicates that no extra porosity is formed due to the presence of titania nanoparticles on the external surface. So one can conclude from N_2-sorption isotherms that the maximum loading capacity of titania nanoparticles inside the mesopores depends upon the porous characteristics of the silica support material.

3.2.2. Transmission electron microscopy

The shape of the nitrogen sorption isotherms gives an estimate about the location of the titania nanoparticles in the mesoporous support materials. More detailed information on this issue can be deduced from TEM measurements. TEM images of SBA sc-3-2 and SBA scs-3-2 are shown in Fig. 5. The results of the TEM analysis of SBA-3-2 and MCF-3-2 are similar to these. Here (Fig. 5a), the overgrowth of titania on the external surface of short-channel SBA can be clearly seen (indicated by a white arrow). Fig. 5b shows the results of a HAADF measurement of SBA sc-3-2. The contrast strongly depends on the *Z*-number (the technique is also called *Z*-contrast imaging) and therefore titania appears as a brighter contrast region (indicated by a white arrow) in the silica matrix. The presence of titania nanoparticles inside the mesopores is clearly observed due to the appearance of a grey contrast in the pores. These results confirm the indications given by nitrogen sorption isotherms for SBA sc-3-2 indicating the presence of titania both in the porous matrix and on the external surface.

A TEM image of the sample SBA scs-3-2 is shown in Fig. 5c. In this image, one can clearly see the large pores of this type of material induced by the addition of the swelling agent. Moreover, overgrowth of titania nanoparticles at the external surface, such as in Fig. 5a, was not observed. *Z*-contrast imaging was also performed on this sample. The titania located in the mesopores, however, could not be detected due to the more complex pore structure of the mesoporous support material. This implies that TEM could not present a direct proof that the titania nanoparticles are only present at the internal surface of the silica support.

3.3. Photocatalytic activity of the catalysts

As generally known, only the anatase crystal phase of titania shows good photocatalytic behavior as well as mixtures of anatase with small amounts of rutile or brookite. Therefore, the crystal phase of the catalyst was determined with FT-Raman spectroscopy (Fig. 6). All the catalysts show similar bands at 640, 520, 400 and 150 cm^{-1}. These bands confirm that the crystal phase of the titania present in the porous structure consists of pure anatase. The performance of the catalysts has been studied with two different catalytic setups. One setup is a commonly used test reaction where organic coloring agents are degraded in aqueous environment under UV irradiation. The degradation of the organic compound can be followed by the decrease in absorbance in UV–vis spectroscopy. The second setup is a continuous flow setup in gaseous environment. Here, the degradation of a continuous ethanol flow has been evaluated with on line gas chromatography.

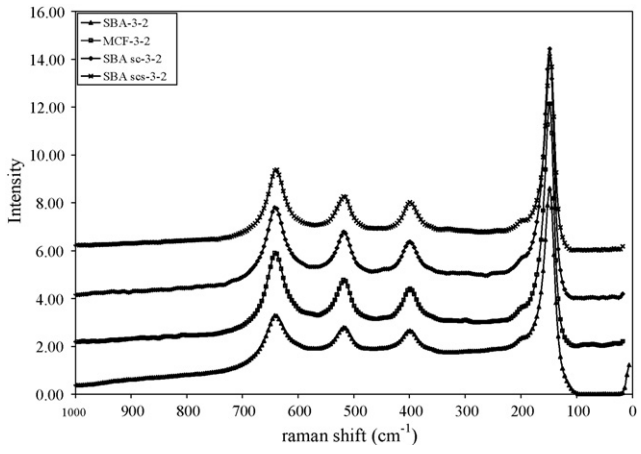

Fig. 6. FT-Raman spectra of the catalysts. All four catalysts show typical bands of anatase. Offsett = 2.

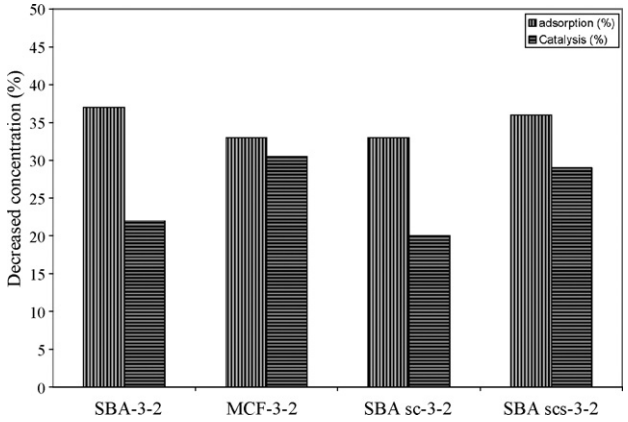

Fig. 7. Adsorption and photocatalytic activity of the catalysts in aqueous phase. Results shown in percentages of adsorption and catalysis.

3.3.1. Photocatalytic activity in aqueous environment

The results of the photocatalytic test reaction in aqueous environment, as described in the experimental, are shown in Fig. 7. The difference in adsorption capacity and catalytic activity between the various samples can be clearly seen. The differences in adsorption capacity between the catalysts seem to be related to the differences in textural characteristics. The materials with high specific surface area or pore volumes show higher adsorption capacities. Therefore, SBA-3-2 (with the highest specific surface area) and SBA scs-3-2 (with the lowest specific surface area but a significantly higher pore volume) have a higher adsorption capacity compared to SBA sc-3-2 and MCF-3-2. When the photocatalytic activity of the catalysts is compared, the pore size becomes more important. The MCF-type catalysts (MCF-3-2 and SBA scs-3-2) are found to be much more active compared to the materials prepared in the absence of swelling agents. Indeed, MCF-type materials contain larger pores and therefore, all active titania sites will be better accessible for the large organic compound. Moreover, larger pore sizes allow higher mass transfers. SBA and SBA sc on the other hand, possess smaller pores that are partially narrowed or blocked after deposition of the titania nanoparticles. Because of these narrowed pores, diffusion limitations can arise that prevent a certain amount of titania to be reached by the organic dye [41]. Therefore, the smaller pore size in the SBA and SBA sc materials cause a significant decrease in the photocatalytic degradation of large organic dyes. These observations suggest that liquid phase photocatalytic degradation depends to a great extend on the structural characteristics of the catalyst and diffusion effects that are related to them.

3.3.2. Photocatalytic activity in gaseous environment

The photocatalytic activity in the gas phase was tested in continuous mode with ethanol as representative VOC. The catalytic setup is shown in Fig. 8. In a first step, a flow of 1000 ml air per minute containing 250 ppm ethanol is applied. This initial flow

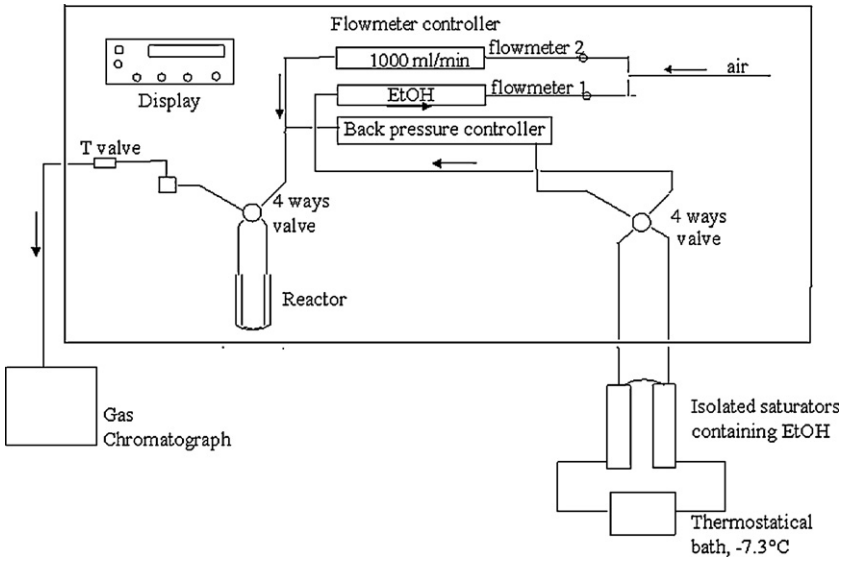

Fig. 8. Flow scheme of the continuous flow setup.

goes directly to the GC without passing the reactor. When the GC signal is stabilized (Fig. 9, part 1), the valve is switched so that the flow passes through the quartz reactor, containing 0.1 g of catalyst. At this point, the adsorption of ethanol on the catalyst begins (Fig. 9, part 2). The catalyst is completely saturated with ethanol, when the initial flow is regained. Once saturated, the catalyst is illuminated with UV-light to start the photodegradation of ethanol. Due to the heat of the lamp, there is first a slight desorption of the adsorbed ethanol. Afterwards, a decrease of ethanol is observed due to the photodegradation (Fig. 9, part 3). After a certain time, an equilibrium between the amount of ethanol in the flow and the photodegradation is obtained. Here, the effectiveness of the photodegradation of the catalyst in the continuous flow catalytic setup can be calculated.

Table 2 shows the results of the catalysts tested in the above described continuous flow test setup. The differences between the various catalysts are not high but still significant. The catalysts MCF-3-2 and SBA scs-3-2 show better activity compared to SBA-3-2 and SBA sc-3-2. In addition, SBA-3-2 shows the lowest activity which can be caused by the longer mesoporous channels of up to several micrometers in length (Fig. 3b.) as well as the smallest pore diameter. These results are similar to those obtained via the photocatalytic test reaction in aqueous phase. However, the photocatalytic activity is quite low compared to the liquid phase. It should be mentioned that only small amounts of catalyst were used and that the test setup worked with a high continuous flow (1000 ml/min) of ethanol.

This means that the contact times on the catalyst are quite small (seconds compared to tens of minutes in the liquid phase). The short contact times result in lower catalytic conversions. Nevertheless it is clear that the same trend as in liquid phase catalysis can be observed. All of the samples contain similar amounts of titania. Therefore, differences in catalysis are originating from the samples porous and morphological characteristics. Fig. 10 shows the adsorption kinetics of pure ethanol on the different catalysts. It can be clearly seen that the adsorption of ethanol is much faster on the catalysts with large pore diameters, more open structures and smaller particle sizes. Adsorption/desorption equilibrium on MCF-3-2 and SBA scs-3-2 are reached within 1 and 3 min, respectively, in contrast to SBA sc-3-2 and SBA-3-2 that need more than 6 and

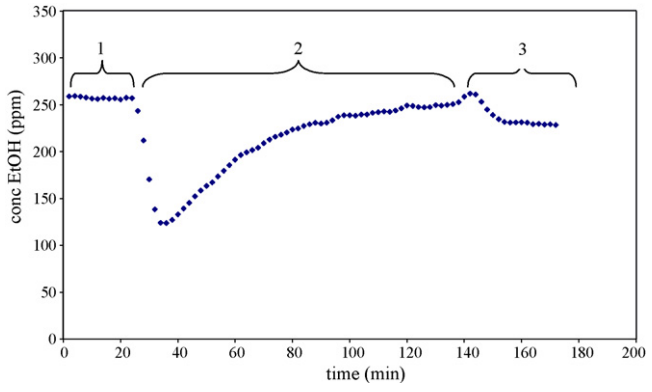

Fig. 9. Photodegradation of ethanol with MCF-3-2 under continuous flow of ethanol. (1) Initial baseline, (2) saturation of MCF-3-2 with ethanol and (3) photodegradation of ethanol.

Table 2
Results of the photodegradation of ethanol by the different catalysts

	SBA-3-2	SBA sc-3-2	MCF-3-2	SBA scs-3-2
Initial concentration (ppm)	246.5	251.0	243.0	249.0
Degraded concentration (ppm)	14.0	17.5	20.0	19.5
Catalysis (%)	5.7	6.9	8.3	7.8

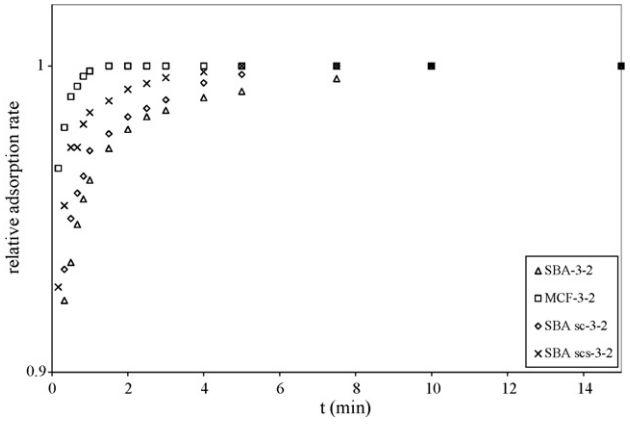

Fig. 10. Adsorption kinetics of the different catalysts.

8 min, respectively, to attain equilibrium. The MCF-3-2 and SBA scs-3-2 catalysts are more easily accessible to molecules and allow higher mass transfers giving rise to increased catalytic degradation compared to the materials with smaller pore diameters, longer pores and smaller particle sizes. It is clear that the morphology of the silica support plays an essential role in the catalytic performance of these materials.

4. Conclusions

In this work, the influence of the morphology of the support on the deposition of titania and on the photocatalytic activity is discussed. For applications in textile industry, several demands are requested for the catalyst. The particle size of the support materials has to be less then 2 μm in order to fit into the textile fibers. Also for paint and wallpaper applications the size of the particles should be as small as possible. Therefore, materials with adjusted particle sizes that fulfill the demands of the textile industry were synthesized (SBA sc and SBA scs). A second requirement is the inactivity of the external surface of the catalyst to prevent degradation of the textile and its color. It was found that the pore size of the support is important to prevent deposition on the external surface. As discussed, after deposition of titania on SBA and SBA sc, overgrowth of titania on the external surface is obtained. MCF-3-2 and SBA scs-3-2, however, show no overgrowth in N_2-sorption isotherms and in TEM. Therefore, the titania particles will most likely be deposited inside the mesopores. It can be concluded that the catalyst SBA scs-3-2 shows interesting characteristics for use in the textile industry.

The morphology of the particles, length of the pore channels and pore sizes proved very important towards the catalytic performance of the materials. In aqueous phase, MCF-3-2 and SBA scs-3-2 show better photodegradation of rhodamine-6G compared to SBA-3-2 and SBA sc-3-2. These results suggest a better accessibility of the titania for the organic compound due to the larger pores of MCF and SBA scs. These results are also confirmed by the continuous gas phase test setup. Taking in mind the small amounts of catalyst and the high continuous flow (1000 ml/min), the catalysts show rather high activities under continuous flow photodegradation. From both liquid phase and gas phase catalysis it is clear that the porous characteristics and the morphological features have an important influence on preventing the deposition of active elements on the external surface and on the catalytic performance. In addition it can be mentioned that these type of materials, and in specific SBA scs-3-2, are interesting to use in textile industry.

Acknowledgements

The Inside Pores Network of Excellence (NOE), the Concerted Research Project (CRP) sponsored by the Special Fund for Research at the UA, the Belgian Textile Research Center (Centexbel), the Institute for the Promotion of Innovation by Science and Technology in Flanders (IWT) (project no. 30916) and the Ministerio de Educación y Ciencia (Spain, Project NAN2004-09267-C03) are gratefully acknowledged. V. Meynen is thankful to the FWO-Flanders for her research grant.

References

[1] S. Gupta, M. Khare, R. Goyal, Building and Environment 42 (2007) 2797.
[2] P.S. Hui, L.T. Wong, K.W. Mui, Building and Environment 42 (2007) 2900.
[3] C.G. Helmis, J. Tzoutzas, H.A. Flocas, C.H. Halios, O.I. Stathopoulou, V.D. Assimkopoulos, V. Panis, M. Apostolatou, G. Sgouros, E. Adam, Science of the Total Environment 377 (2007) 349.
[4] A.P. Jones, Atmospheric Environment 14 (1997) 117.
[5] J. Sundell, ASHRAE Journal June (1996) 51.
[6] J.A. Hoskins, Indoor and Built Environment 12 (2003) 427.
[7] R.M. Alberici, W.E. Jardim, Applied Catalysis B: Environmental 14 (1997) 55.
[8] J.F. San Jose-Alonso, E. Velasco-Gomez, F.J. Rey-Martinez, M. Alvarez-Guerra, C. Gallego-Pelaez, Energy Build 29 (1999) 179.
[9] L. Morawska, Indoor Air 16 (2006) 335.
[10] B.W. Olesen, Energy and Buildings 39 (7) (2007) 740.
[11] S. Wang, H.M. Ang, M.O. Tade, Environmental International 33 (2007) 694.
[12] J. Van Durme, J. Dewulf, W. Sysmans, C. Leys, H. Van Langenhove, Applied Catalysis B: Environmental 74 (2007) 161.
[13] U. Diebold, Surface Science Reports 48 (2003) 53.
[14] A.L. Linsebigler, G. Lu, J.T. Yates Jr., Chemical Reviews 95 (1995) 735.
[15] A. Fujishima, K. Hashimoto, T. Watanabe, TiO_2 Photocatalysis Fundamentals and Applications, BKC, Inc., Tokyo, 1999.
[16] M. Daté, Y. Ichihashi, T. Yamashita, A. Chiorino, F. Boccuzzi, M. Haruta, Catalysis Today 72 (2002) 89.
[17] W.K. Jo, K.H. Park, Chemosphere 57 (2004) 555.
[18] W.H. Ching, M. Leung, D.Y.C. Leung, Solar Energy 77 (2004) 129.
[19] L. Yang, Z. Liu, J. Shi, Y. Zhang, H. Hu, W. Shangguan, Separation and Purification Technology 54 (2007) 204.
[20] K. De Witte, P. Cool, I. De Witte, L. Ruys, J. Rao, G. Van Tendeloo, E.F. Vansant, Journal of Nanoscience and Nanotechnology 7 (2007) 2511.
[21] D. Zhao, J. Feng, Q. Huo, N. Melosh, G.H. Fredrickson, B.F. Chmelka, G.D. Stucky, Science 279 (1998) 548.
[22] D. Zhao, Q. Huo, J. Feng, B.F. Chmelka, G.D. Stucky, Journal of the American Chemical Society 120 (1998) 6024.
[23] S.Z. Qiao, H. Djojoputro, Q. Hu, G.Q. Lu, Progress in Solid State Chemistry (2005) 1.
[24] A. Sayari, B.-H. Han, Y. Yang, Journal of the American Chemical Society 126 (2004) 14348.
[25] C. Yu, J. Fan, B. Tian, D. Zhao, G.D. Stucky, Advanced Materials 23 (2002) 1742.
[26] P. Schmidt-Winkel, W.W. Lukens, D. Zhao, P. Yang, B.F. Chmelka, G.D. Stucky, Journal of the American Chemical Society 121 (1999) 254.
[27] P. Schmidt-Winkel, W.W. Lukens, P. Yang, D.I. Margolese, J.S. Lettow, J.Y. Ying, G.D. Stucky, Chemistry of Materials 12 (2000) 686.
[28] L. Wang, T. Qi, Y. Zhang, J. Chu, Microporous and Mesoporous Materials (2006) 156.
[29] M.M. Mohamed, T.M. Salama, T. Yamaguchi, Colloids and Surfaces A: Physicochemical and Engineering Aspects 207 (2002) 25.
[30] W. Wang, M. Song, Materials Research Bulletin 41 (2006) 436.
[31] S. Perathoner, P. Lanzafame, R. Passalacqua, G. Centi, R. Schlögl, D.S. Su, Microporous and Mesoporous Materials 90 (2006) 347.
[32] A. Sayari, Chemistry of Materials 8 (1996) 1840.
[33] K. Moller, T. Bein, Chemistry of Materials 10 (1998) 2950.
[34] Y. Chen, Y. Huang, J. Xiu, X. Han, X. Bao, Applied Catalysis A: General 273 (2004) 185.
[35] P.V. Messina, P.C. Schulz, Journal of Colloid and Interface Science 299 (2006) 305.
[36] T. Hoshikawa, T. Ikebe, M. Yamada, R. Kikuchi, K. Eguchi, Journal of Photochemistry and Photobiology A: Chemistry 184 (2006) 78.
[37] J. Jiménez-Jiménez, M. Rubio-Alonso, D. Eliche-Quesada, E. Rodriguez Castellon, A. Jiméne-Lopez, Journal of Physics and Chemistry of Solids 67 (2006) 1007.
[38] A. Bhattacheryya, S. Kawi, M.B. Ray, Catalysis Today 98 (2004) 431.
[39] P. Van Der Voort, P.I. Ravikovitch, K.P. De Jong, A.V. Neimark, A.H. Janssen, M. Benjelloun, E. Van Bavel, P. Cool, B.M. Weckhuysen, E.F. Vansant, Chemical Communications (2002) 1010.
[40] A.M. Busuioc, V. Meynen, E. Beyers, M. Mertens, P. Cool, N. Bilba, E.F. Vansant, Applied Catalysis A: General 312 (2006) 153.
[41] V. Meynen, Y. Segura, M. Mertens, P. Cool, E.F. Vansant, Microporous and Mesoporous Materials 85 (2005) 119.